Supporting Information

Flexible Point-of-Use Phosphate Electrochemical Sensors Based on Electrodeposited Molybdenum Oxide

Siqi Yu,[a] Xiyu Sun,[a] Zinan Yu,[b] Jinwook Jung,[c] Satoshi Ishii,[d] Christopher T. Hayes,[e] Valérie C. Pierre,[b] Amar Flood,[f] Jason D. Azoulay,[g] and Tse Nga Ng*[a,c]

[a] Department of Electrical and Computer Engineering, University of California San Diego, La Jolla, CA 92093, USA

[b] Department of Chemistry, The University of Utah, Salt Lake City, UT 84112, USA

[c] Program in Materials Science and Engineering, University of California San Diego, La Jolla, CA 92093, USA

[d] Department of Soil, Water, and Climate, University of Minnesota, St. Paul, MN 55108, USA

[e] School of Ocean Science and Engineering, University of Southern Mississippi, Stennis Space Center, MS 39529, USA

[f] Department of Chemistry, Indiana University, Bloomington, IN 47405, USA

[g] School of Chemistry and Biochemistry and School of Materials Science and Engineering, Center for Organic Photonics and Electronics, Georgia Institute of Technology, Atlanta, GA 30332, USA

*Email: tnn046@ucsd.edu

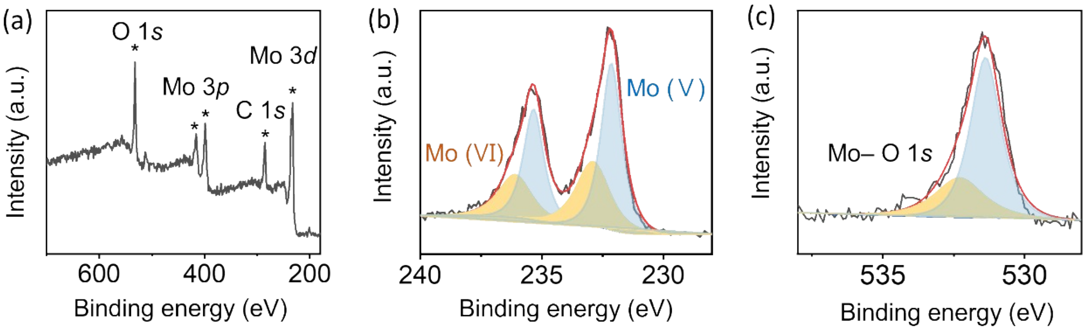

Figure S1. (a) X-ray photoelectron spectroscopy spectra (XPS) of the electrodeposited MoO_x sample. (b) High-resolution XPS at Mo 3*d* orbital. (c) High-resolution XPS at O 1*s* orbital. The peaks in orange and blue colors indicate the data fitting corresponding to Mo(VI) and Mo(V), respectively.

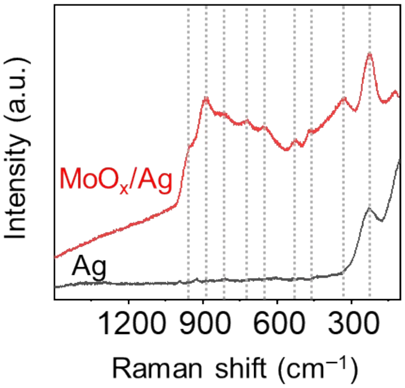

Figure S2. Raman spectra of silver substrate (black line) and electrodeposited MoO_x on silver (red line). The peak positions indicated by the dashed lines are 960, 890, 818, 727, 654, 525, 462, 334 and 226 cm^{-1}, respectively. Raman spectra were collected using a Renishaw inVia upright microscope equipped with a 785 nm excitation laser (50% power), with two accumulated exposures and an exposure time of 10 s each.

The peak at 226 cm^{-1} corresponds to vibrational mode of Ag and oxygen due to the adsorbed oxygen (Ref.S1). The Raman bands at 818, 654 and 334 cm^{-1} are attributed to MoO_3, corresponding to the stretching and bending modes of Mo–O bonds (Refs. S1,S2). The band at 727 cm^{-1} is characteristic of MoO_2 (Ref. S2). The bridging Mo–O–Mo corresponds to bands at 525 and 462 cm^{-1}. The peaks at 960 and 890 cm^{-1}, associated with Mo–O vibrations, are not characteristic of either MoO_3 or MoO_2, but may instead indicate the presence of intermediate mixed-valence molybdenum oxides such as Mo_4O_{11} (Ref. S2).

The Raman signal of MoO_x is not a simple superposition of the characteristic peaks of MoO_3 and MoO_2, but instead present some new peaks and broadened and asymmetric bands. This indicates that the electrodeposited MoO_x is not a physical mixture of MoO_3 and MoO_2, but rather a disordered molybdenum oxide with mixed valence (+5 and +6), so the Mo–O bonding environments are very complicated and lead to broadened Raman features.

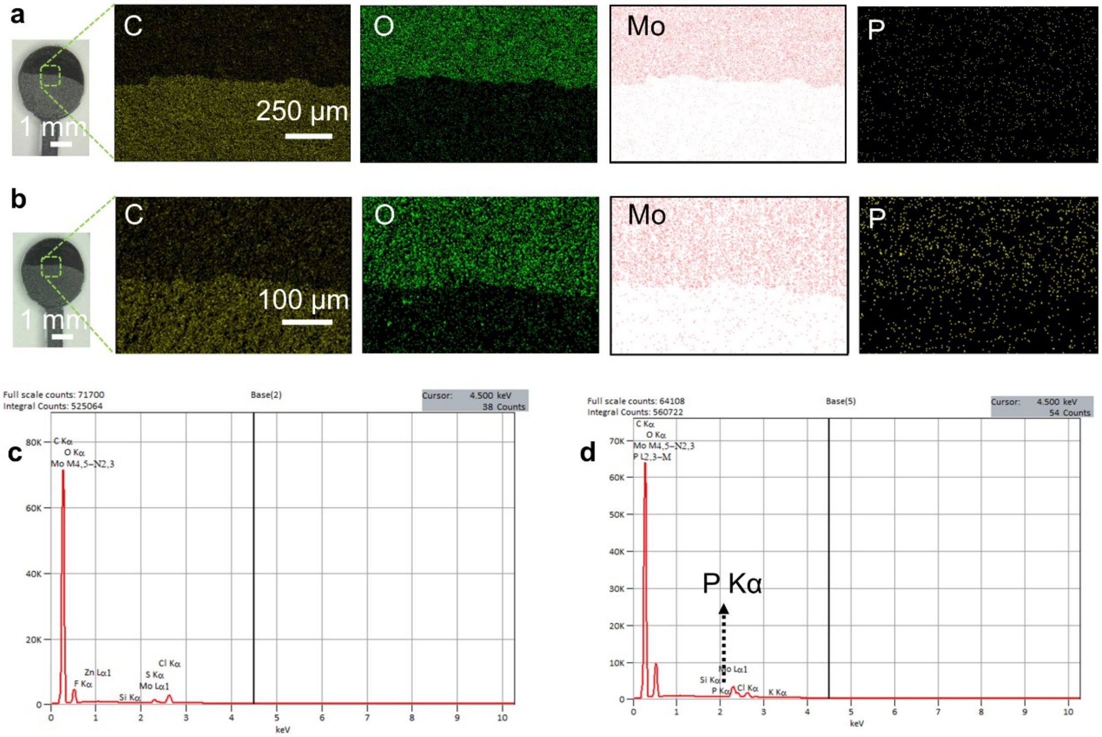

Figure S3. Energy-dispersive x-ray spectroscopy mapping for C, O, Mo and P elements of (a and c) MoO_x and (b and d) MoO_x-phospohate.

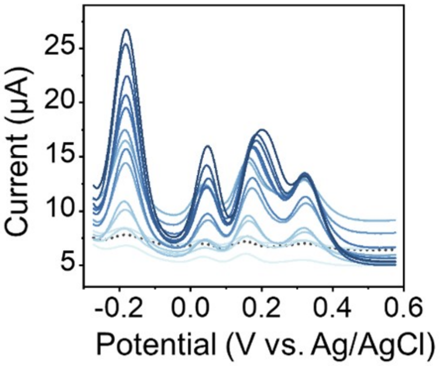

Figure S4. Square wave voltammetry (SWV) data of Fig. 2d, with increasing phosphate concentrations ranging from 0.1 μM to 10 mM, as collected before any baseline adjustment.

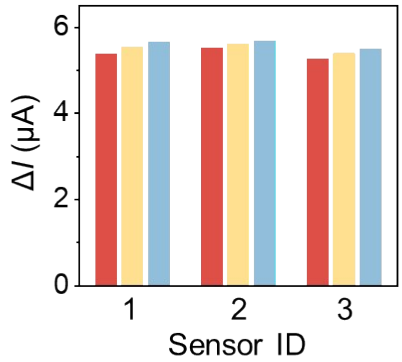

Figure S5. Current changes of three independently fabricated MoO_x sensors recorded in three consecutive measurements at 12 min (red), 13 min (yellow), and 14 min (blue) after addition of 100 μM phosphate, showing sensor-to-sensor reproducibility and measurement stability of individual MoO_x sensor.

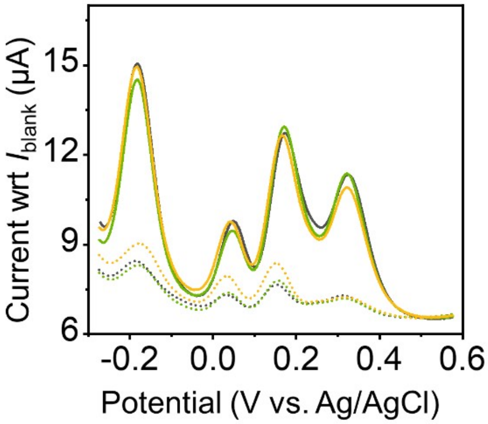

Figure S6. SWV data in the presence (solid lines) and absence (dotted lines) of 100 μM phosphate, with additional anions of 1 mM CO_3^{2-} (green lines) or SiO_3^{2-} (yellow lines). The lines in black denote initial measurements without additional anions.

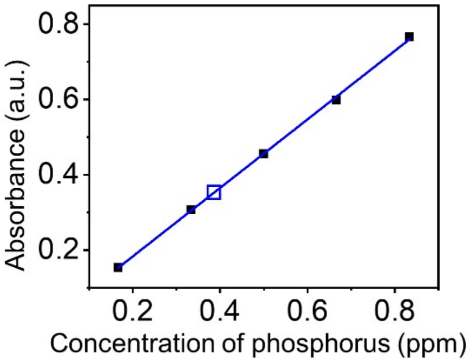

Figure S7. Calibration curve for the conventional molybdenum blue colorimetric assay at 820 nm with the fitted equation absorbance = 0.91 × [phosphorus in ppm] + 0.00072. The absorbance corresponding to the wastewater influent sample is denoted by the square symbol. Molybdenum blue analysis was conducted by mixing 0.5 mL of influent sample with 1.5 mL deionized water and 1 mL reagent solution. The reagent solution was prepared by mixing deionized water, 10 wt% ascorbic acid, 2.5 wt% ammonium paramolybdate tetrahydrate, and 3 M sulfuric acid in a 2:1:1:1 volume ratio. The mixture was incubated at 37 °C for 90 minutes prior to UV-Visible absorption analysis. Since the sample was diluted 1:6 by volume with the reagent solution, the concentration in the plot is multiplied by 6 fold to reach the original concentration of 2.3 ppm.

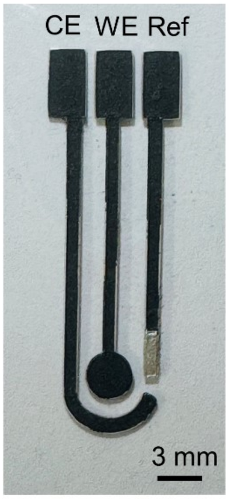

Figure S8. Photograph of the stencil-printed sensor electrodes fabricated on a plastic substrate, with graphite as the working and counter electrodes, and Ag/AgCl ink as the reference electrode.

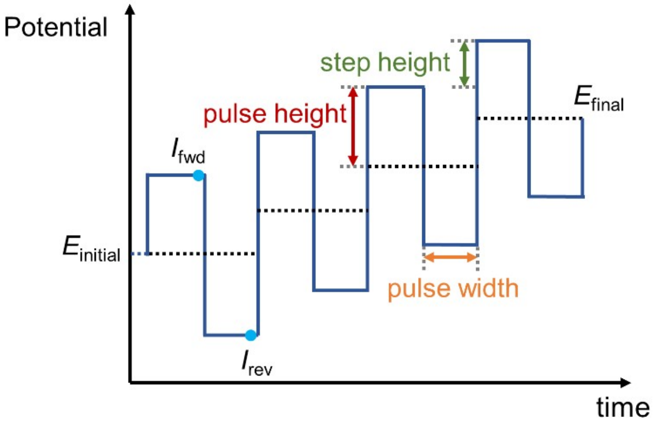

Figure S9. The concept diagram of SWV. This work uses a pulse height of 25 mV, a step height of 1 mV, and a pulse width of 10 ms, scanned from −0.27 V to 0.57 V in 0.1 M KCl and 0.1 M H_2SO_4 or −0.14 V to 0.67 V in 1 M KCl and 0.1 M H_2SO_4.

Table S1. Summary of electrochemical redox peaks reported for molybdate-based materials.*

Material	**Method**	**Peak potential** #	**Assignment**	**Ref.**
$[\mathrm{PMo}^{(\mathrm{VI})}_{12}\mathrm{O}_{40}]^{3-}$	SWV	0.10 V	$[\mathrm{H}_2\mathrm{PMo}^{(\mathrm{V})}_{2}\mathrm{Mo}^{(\mathrm{VI})}_{10}\mathrm{O}_{40}]^{3-} \leftrightarrow [\mathrm{H}_5\mathrm{PMo}^{(\mathrm{V})}_{5}\mathrm{Mo}^{(\mathrm{VI})}_{7}\mathrm{O}_{40}]^{3-}$	S4
		0.26 V	$[\mathrm{PMo}^{(\mathrm{VI})}_{12}\mathrm{O}_{40}]^{3-} \leftrightarrow [\mathrm{H}_2\mathrm{PMo}^{(\mathrm{V})}_{2}\mathrm{Mo}^{(\mathrm{VI})}_{10}\mathrm{O}_{40}]^{3-}$	
$[\mathrm{PMo}^{(\mathrm{VI})}_{12}\mathrm{O}_{40}]^{3-}$	CV	–0.03 V	$[\mathrm{PMo}^{(\mathrm{V})}_{4}\mathrm{Mo}^{(\mathrm{VI})}_{8}\mathrm{O}_{40}]^{7-} \leftrightarrow [\mathrm{PMo}^{(\mathrm{V})}_{6}\mathrm{Mo}^{(\mathrm{VI})}_{6}\mathrm{O}_{40}]^{9-}$	S5
		0.20 V	$[\mathrm{PMo}^{(\mathrm{V})}_{2}\mathrm{Mo}^{(\mathrm{VI})}_{10}\mathrm{O}_{40}]^{5-} \leftrightarrow [\mathrm{PMo}^{(\mathrm{V})}_{4}\mathrm{Mo}^{(\mathrm{VI})}_{8}\mathrm{O}_{40}]^{7-}$	
		0.35 V	$[\mathrm{PMo}^{(\mathrm{VI})}_{12}\mathrm{O}_{40}]^{3-} \leftrightarrow [\mathrm{PMo}^{(\mathrm{V})}_{2}\mathrm{Mo}^{(\mathrm{VI})}_{10}\mathrm{O}_{40}]^{5-}$	
$[\mathrm{PMo}^{(\mathrm{VI})}_{12}\mathrm{O}_{40}]^{3-}$	CV	0.10 V	$[\mathrm{PMo}^{(\mathrm{VI})}_{12}\mathrm{O}_{40}]^{3-} \leftrightarrow [\mathrm{Mo}^{(\mathrm{VI})}_{7}\mathrm{O}_{24}]^{6-}$	S6
		0.25 V	$\mathrm{H}^{+} \leftrightarrow H_2\mathrm{O}$	
$\mathrm{Mo}_x\mathrm{O}_y\text{-}\mathrm{PO}_4^{3-}$	SWV	–0.03 V	$\mathrm{Mo}^{(\mathrm{II})} \leftrightarrow \mathrm{Mo}^{(\mathrm{IV})}$	S7
		0.20 V	$\mathrm{Mo}^{(\mathrm{IV})} \leftrightarrow \mathrm{Mo}^{(\mathrm{VI})}$	
$[\mathrm{PMo}^{(\mathrm{VI})}_{12}\mathrm{O}_{40}]^{3-}$	CV	–0.07 V	$\mathrm{Mo}^{(\mathrm{V})} \leftrightarrow \mathrm{Mo}^{(\mathrm{VI})}$	S8
		0.10 V	$\mathrm{Mo}^{(\mathrm{V})} \leftrightarrow \mathrm{Mo}^{(\mathrm{VI})}$	
$\mathrm{K}^{\mathrm{W9Mo2}}{}_{\mathrm{Sn}}$	CV	–0.51 V	No specific oxidation state assignment	S9
		–1.13 V		

CV: cyclic voltammetry; $\mathrm{Mo}_x\mathrm{O}_y$: Mixed-valent molybdenum oxide; $\mathrm{K}^{\mathrm{W9Mo2}}{}_{\mathrm{Sn}}$: $(\mathrm{TBA})_4[\mathrm{PW}_9\mathrm{Mo}_2\mathrm{O}_{39}\{\mathrm{Sn}(\mathrm{C}_6\mathrm{H}_4\mathrm{I})\}]$.

*It should be noted that the literature reported varying results, and the definitive peak assignments remain uncertain. But we try to summarize representative interpretations based on selected studies.
#All peak potentials were converted to values versus Ag/AgCl (saturated KCl) reference electrode.

Table S2. Performance of molybdate-based electrochemical sensors for phosphate detection.

Electrode	Method	Linear range (μM)	Sensitivity μA μM^{-1}	Sensitivity μA dec^{-1} *	Reference
Mo_xO_y/PDAAQ/GCE	SWV	0.03–4	0.711	1.33	S7
ZrO_2/ZnO/MWCNTs/AMT/SPE	CV	0.037–1.1	86.7	64.9	S8
AMT/AgNWs/SPE	CV	5–1000	0.71	252	S10
MoP-PGE	DPV	10–100	0.0381	3.43	S11
Au wire	DPV	0.1–50	0.0033	0.061	S12
AMT-CS-GCE	SWV	0.3–2	4.38	9.04	S13
PVC/MB/PGE	DPV	0.03–1	3.27	2.08	S14
MoO_x/SPE	SWV	8–1000	Not applicable	5.09	this work

PDAAQ: Poly 1,2-diaminoanthraquinone; GCE: glassy carbon electrode; SPE: screen printed electrode; AMT: ammonium molybdate tetrahydrate; AgNWs: silver nanowires; MWCNTs: multi-wall carbon nanotubes; MoP-PGE: molybdenum phosphate coated pencil graphite electrode; DPV: differential pulse voltammograms; CS: chitosan; PVC: poly(vinyl chloride); MB: molybdenum blue; PGE: pencil graphite electrode.

*The sensitivities in μA dec^{-1} were estimated from the respective calibration plot in each reference.

In Refs. S8, S10, S12, and S13, the ammonium molybdate (AMT) solution was dropcasted onto the electrode surface and dried to fabricate the sensors. While the initial sensitivity could be high, the molybdate was observed to redissolve during measurement, and the degree of dissolution depends on film thickness, drying conditions, and electrolyte composition, which lead to signal instability and poor reproducibility.

In Ref. S11, the phosphate was already introduced into the sensor during fabrication, which occupies some binding sites in advance. This reduced the number of available sites for target phosphate and introduced significant background signals, ultimately resulting in low sensitivity and a low upper detection limit.

While Ref. S7 and S14 adopted more stable solid-state sensing films, they required more complex surface modifications such as in-situ polymerization or polymer coatings to get satisfied performances, and the wetting of aqueous solutions on a hydrophobic polymer surface would present challenges and hence lower sensitivity than our sensor, which was based on an electrochemically deposited mixed-valence MoO_x film that formed an insoluble and well-adhered layer with a simple fabrication process.

References

(1) Millar·, G. J.; Nelson, M. L.; Uwins, P. J. R. *A Combined Environmental Scanning Electron Microscopy and Raman Microscopy Study Ofmethanol Oxidation on Silver(I) Oxide*; 1997; Vol. 43.

(2) Tian, H.; Roberts, C. A.; Wachs, I. E. Molecular Structural Determination of Molybdena in Different Environments: Aqueous Solutions, Bulk Mixed Oxides, and Supported MoO3 Catalysts. *Journal of Physical Chemistry C* **2010**, *114* (33), 14110–14120. https://doi.org/10.1021/jp103269w.

(3) Dieterle, M.; Mestl, G. Raman Spectroscopy of Molybdenum Oxides: Part II. Resonance Raman Spectroscopic Characterization of the Molybdenum Oxides Mo4O11 and MoO2. *Physical Chemistry Chemical Physics* **2002**, *4* (5), 822–826. https://doi.org/10.1039/b107046k.

(4) Barus, C.; Romanytsia, I.; Striebig, N.; Garçon, V. Toward an in Situ Phosphate Sensor in Seawater Using Square Wave Voltammetry. *Talanta* **2016**, *160*, 417–424. https://doi.org/10.1016/j.talanta.2016.07.057.

(5) Tanaka, N.; Unoura, K.; Itabashi, E. *Contribution from the Voltammetric and Spectroelectrochemical Studies of 12-Molybdophosphoric Acid in Aqueous and Water-Dioxane Solutions at a Gold-Minigrid Optically Transparent Thin-Layer Electrode*; 1982; Vol. 21. https://pubs.acs.org/sharingguidelines.

(6) Tang, C.; Fu, D.; Wang, R.; Zhang, X.; Wei, L.; Li, M.; Li, C.; Cao, Q.; Chen, X. An Electrochemical Microfluidic System for On-Site Continuous Monitoring of Soil Phosphate. *IEEE Sens J* **2024**, *24* (5), 6754–6764. https://doi.org/10.1109/JSEN.2023.3348807.

(7) Altahan, M. F.; AbdelAzzem, M. A New Approach for Determination of Orthophosphate Based on Mixed Valent Molybdenum Oxide/Poly 1,2-Diaminoanthraquinone in Seawater. *Sci Rep* **2023**, *13* (1). https://doi.org/10.1038/s41598-023-40479-w.

(8) Lu, Y.; Lan, Q.; Zhang, C.; Liu, B.; Wang, X.; Xu, X.; Liang, X. Trace-Level Sensing of Phosphate for Natural Soils by a Nano-Screen-Printed Electrode. *Environ Sci Technol* **2021**, *55* (19), 13093–13102. https://doi.org/10.1021/acs.est.1c05363.

(9) Laurans, M.; Mattera, M.; Salles, R.; K'Bidi, L.; Gouzerh, P.; Renaudineau, S.; Volatron, F.; Guillemot, G.; Blanchard, S.; Izzet, G.; Solé-Daura, A.; Poblet, J. M.; Proust, A. When Identification of the Reduction Sites in Mixed Molybdenum/Tungsten Keggin-Type Polyoxometalate Hybrids Turns Out Tricky. *Inorg Chem* **2022**, *61* (20), 7700–7709. https://doi.org/10.1021/acs.inorgchem.2c00866.

(10) Kabir, M. F.; Rahman, M. T.; Gurung, A.; Qiao, Q. Electrochemical Phosphate Sensors Using Silver Nanowires Treated Screen Printed Electrodes. *IEEE Sens J* **2018**, *18* (9), 3480–3485. https://doi.org/10.1109/JSEN.2018.2808163.

(11) Arvas, M. B.; Gürsu, H.; Gençten, M.; Sahin, Y. Electrochemical Formation of Molybdenum Phosphate on a Pencil Graphite Electrode and Its Potential Application for the Detection of Phosphate Ions. *Analytical Methods* **2018**, *10* (35), 4282–4291. https://doi.org/10.1039/c8ay01653d.

(12) Wei, H.; Luan, Y.; Pan, D. All-in-One Portable Microsystem for on-Site Electrochemical Determination of Phosphate in Turbid Coastal Waters. *Microchemical Journal* **2022**, *183*. https://doi.org/10.1016/j.microc.2022.108079.

(13) Lu, Y.; Li, X.; Li, D.; Compton, R. G. Amperometric Environmental Phosphate Sensors. *ACS Sens* **2021**, *6* (9), 3284–3294. https://doi.org/10.1021/acssensors.1c01035.

(14) Arvas, M. B.; Gorduk, O.; Gencten, M.; Sahin, Y. Preparation of a Novel Electrochemical Sensor for Phosphate Detection Based on a Molybdenum Blue Modified Poly(Vinyl Chloride) Coated Pencil Graphite Electrode. *Analytical Methods* **2019**, *11* (30), 3874–3881. https://doi.org/10.1039/c9ay01275c.